JACS
JOURNAL OF THE AMERICAN CHEMICAL SOCIETY

Article

pubs.acs.org/JACS

Dissecting the Molecular Structure of the Air/Water Interface from Quantum Simulations of the Sum-Frequency Generation Spectrum

Gregory R. Medders and Francesco Paesani*

Department of Chemistry and Biochemistry, University of California, San Diego, La Jolla, California 92093, United States

Supporting Information

ABSTRACT: The molecular characterization of the air/water interface is a key step in understanding fundamental multiphase phenomena ranging from heterogeneous chemical processes in the atmosphere to the hydration of biomolecules. The apparent simplicity of the air/water interface, however, masks an underlying complexity associated with the dynamic nature of the water hydrogen-bond network that has so far hindered an unambiguous characterization of its microscopic properties. Here, we demonstrate that the application of quantum many-body molecular dynamics, which enables spectroscopically accurate simulations of water from the gas to the condensed phase, leads to a definitive molecular-level picture of the interface region. For the first time, excellent agreement is obtained between the simulated vibrational sum-frequency generation spectrum and the most recent state-of-the-art measurements, without requiring any empirical frequency shift or ad hoc scaling of the spectral intensity. A systematic dissection of the spectral features demonstrates that a rigorous representation of nuclear quantum effects as well as of many-body energy and electrostatic contributions is necessary for a quantitative reproduction of the experimental data. The unprecedented accuracy of the simulations presented here indicates that quantum many-body molecular dynamics can enable predictive studies of aqueous interfaces, which by complementing analogous experimental measurements will provide unique molecular insights into multiphase and heterogeneous processes of relevance in chemistry, biology, materials science, and environmental research.

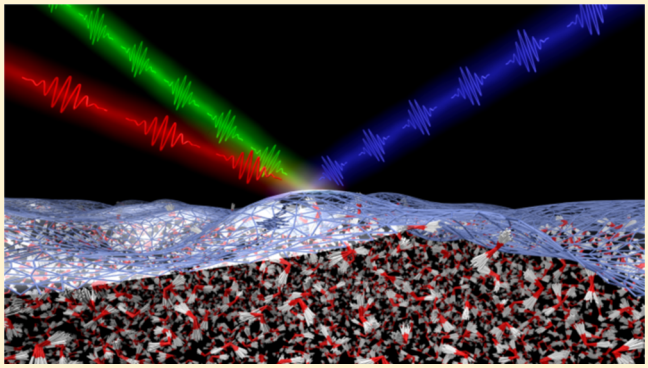

INTRODUCTION

With water covering ~70% of Earth's surface, aqueous interfaces are ubiquitous, mediating many fundamental chemical, physical, biological, and environmental processes.[1−6] The air/water interface of atmospheric aerosol particles regulates the adsorption and reaction of trace gases, which in turn modifies the chemical composition of the particles, with repercussion on climate, the environment, and public health.[7−9] By acting as effective transmission units, interfacial water molecules are part of the recognition process and facilitate the formation of favorable contacts in protein−protein and protein−DNA assemblies.[10] The molecular properties of membrane−water interfaces affect how membrane proteins are anchored to the lipid bilayer,[11] whereas interfacial water molecules in the major and minor grooves are critical to the equilibrium structure and function of DNA.[12,13] Furthermore, interfacial water can act as both solvent and reactant in heterogeneous processes taking place at metal surfaces, including electrolysis, corrosion, and electrocatalysis.[14,15]

There are relatively few experimental techniques capable of probing aqueous interfaces with molecular-level sensitivity. Although some techniques, such as photoelectron spectroscopy,[16] neutron reflectivity,[17] and attenuated total reflection spectroscopy,[18] report on near-surface processes, they are not purely surface specific. In contrast, by measuring the signal generated in the region where the centrosymmetric nature of the solution is broken by the presence of an interface, second-order nonlinear vibrational spectroscopies are (within the electric-dipole approximation) intrinsically surface specific.[19−21] Particularly, vibrational sum-frequency generation (vSFG) spectroscopy,[22] in which a pulsed visible beam is overlapped in space and time with a pulsed infrared (IR) beam to generate a signal at the sum frequency, has emerged as a powerful technique for probing the molecular structure and dynamics of aqueous interfaces.[2,3,5,6,23]

Although HD-vSFG spectra measured for the air/water interface directly probes the molecular properties of the interfacial hydrogen-bonding network, resolving the spectral features into specific structural and dynamical behavior of the water molecules at the surface poses substantial difficulties and is the subject of ongoing debate.[24−42] In this study, we derive a rigorous molecular-level picture of the air/water interface from quantum and classical many-body molecular dynamics (MB-MD) simulations of the corresponding HD-vSFG spectrum. The MB-MD simulations were carried out with the MB-pol

Received: January 25, 2016
Published: March 4, 2016

DOI: 10.1021/jacs.6b00893
J. Am. Chem. Soc. 2016, 138, 3912−3919

potential energy surface, which currently provides the most accurate representation of the interactions between water molecules from the gas to the condensed phase.[43−47] By construction, the MB-MD methodology includes all contributions to the HD-vSFG spectrum from first principles. Specifically, both nuclear quantum effects as well as many-body effects on the underlying interaction energy and electrostatics are explicitly taken into account, enabling a systematic dissection of the individual spectral features in terms of the underlying molecular structure.

BRIEF OVERVIEW OF WHAT IS KNOWN ABOUT THE VSFG SPECTRUM OF THE AIR/WATER INTERFACE

Within vSFG, the structure and dynamics of molecules at the air/water interface is encoded in frequency shifts in the line shape arising from hydrogen bonding. Specifically, vibrational transitions that are resonant with the incident infrared frequency are manifest in the resonant part of the second-order nonlinear susceptibility, $\chi^{(2,R)}$. In the earliest measurements of vSFG spectra of the air/water interface, however, direct measurement of $\chi^{(2,R)}$ was not possible,[24,25] with the measured signal instead being related to the square of the total (resonant and nonresonant) second-order nonlinear susceptibility, $I^{SFG} \approx |\chi^{(2,R)} + \chi^{(2,NR)}|^2$.[48] Interpretation of these conventional vSFG spectra in terms of specific structural arrangements of the water molecules at the interface was therefore complicated by the interference between the resonant and nonresonant components of $\chi^{(2)}$. A more direct connection between the spectral features and the underlying molecular structure of the interface was enabled by the development of experimental techniques capable of measuring the imaginary component of the nonlinear susceptibility itself (commonly referred to as the heterodyne-detected sum-frequency generation, HD-vSFG, spectrum).[27,49,50]

From molecular simulations, the imaginary component of the resonant nonlinear susceptibility can be expressed within the time-dependent formalism as[48]

$$\mathrm{Im}[\chi^{(2,R)}_{ijk}(\omega)] = \mathrm{Im}\left[\frac{i\omega}{k_B T}\int_0^\infty \mathrm{d}t\, e^{-i\omega t}\langle \alpha_{ij}(t)\mu_k(0)\rangle\right] \quad (1)$$

Here, ω is the vibrational frequency, $\chi^{(2,R)}$ is the resonant (vibrationally enhanced) SFG susceptibility, and i, j, and k are the components related to the polarization conditions of the sum-frequency, visible, and IR beams, respectively. In the xxz polarization combination, the sign of $\mathrm{Im}[\chi^{(2,R)}_{ijk}(\omega)]$ is related to the direction of the molecular transition dipoles at a given vibrational frequency, thus allowing for an unambiguous determination of the orientation of the water molecules relative to the interface. Specifically, positive and negative spectral features are associated with water molecules with dipole moments pointing up (i.e., toward the air phase) and down (i.e., toward the bulk liquid phase), respectively. This xxz polarization combination, which will be the focus of the present simulations, is also referred to as the "SSP" polarization combination, where S and P denote beam polarizations parallel and perpendicular to the surface, respectively.

Besides a narrow positive peak at ∼3700 cm^{-1} corresponding to stretching vibrations of dangling OH bonds that point out of the surface (free OH), the HD-vSFG spectrum of the air/water interface is characterized by a broad negative feature between 3200 and 3600 cm^{-1} that is associated with OH stretches of hydrogen-bonded water molecules pointing into the bulk. Within this hydrogen-bonded stretching region, two vibrational bands, commonly labeled as OH(I) and OH(II),[33] can be identified at ∼3250 and ∼3450 cm^{-1}, respectively. The OH(I) band was initially attributed to water molecules in symmetric tetrahedral hydrogen-bonded geometries, referred to as icelike structures, whereas the OH(II) was attributed to hydrogen-bonded water molecules in a liquidlike environment.[23−25] In subsequent measurements of the isotopically diluted (HOD) interface, only a single hydrogen-bonded band was observed at ∼3480 cm^{-1}, suggesting that the distinct OH(I) and OH(II) features found in the HD-vSFG spectra of neat H_2O could arise from the intramolecular anharmonic coupling that is absent in HOD.[33] Independent of isotopic dilution, however, the HD-vSFG spectra exhibited a positive feature, labeled as OH(x), which is located at ∼3100 cm^{-1} in neat H_2O.[29,33]

The positive OH(x) feature was initially assigned to tetrahedrally coordinated water molecules in icelike configurations;[29] however, alternative interpretations of the hydrogen-bonded region of the HD-vSFG spectrum have also been proposed. From classical molecular dynamics (MD) simulations with the empirical E3B water model, it was found that short-range three-body interactions enhance the tetrahedral structure of water at the interface which, in turn, can give rise to the positive OH(x) feature.[32] In contrast, MD simulations with an empirical polarizable water model suggested that the OH(x) feature can arise from OH vibrations of a hydrogen-bond donating water molecule in a strongly hydrogen-bonded pair, resulting in an induced dipole moment on the hydrogen-bond acceptor.[30] It was demonstrated that if the hydrogen-bond accepting water molecule has a free OH pointed out of the surface then a component of its two-body dipole moment can also point out of the surface giving rise to the positive OH(x) feature according to an "anisotropic local field" mechanism.[30]

Subsequent MD simulations of the HD-vSFG spectrum of the air/water interface based on density functional theory (DFT) have led to conflicting results. Although purely DFT-based framework based on maximally localized Wannier functions and including quadrupolar contributions have been employed for the calculation of the HD-vSFG spectrum of the ice I_h basal surface,[51] direct DFT simulations of the HD-vSFG spectrum of the air/water interface were found to be not feasible because of their prohibitive computational cost. By employing an approximate treatment of the dipole-polarizability time-correlation function, simulations with the BLYP-D2 functional were found to predict the presence of the positive OH(x) feature at ∼3100 cm^{-1};[36] however, the accuracy of these early results is limited by the very short simulation time employed in these calculations. Recently, rather than calculating the dipole-polarizability time-correlation function directly, Ohto et al. recast eq 1 into a more rapidly converging surface-specific velocity−velocity correlation function (ssVVCF).[52] Although this approach was shown to agree well with the reference values obtained from the dipole-polarizability TCF from an empirically parametrized polarizable force field (POLI2VS),[53] the approximations necessary for the reformulation of eq 1 into the ssVVCF rely upon a simplified description of the system's dipole and polarizability. For this reason, although the HD-vSFG spectra calculated using DFT functionals similar to those of ref 36 (i.e., BLYP-D3, PBE-D3, and revPBE-D3) show no positive OH(x) feature in the HD-vSFG spectrum of the air/water interface,[52] the approximate treatment of the environmental dependence of the dipole

DOI: 10.1021/jacs.6b00893
J. Am. Chem. Soc. 2016, 138, 3912−3919

severely limits the ability of this approach to test the validity of the proposed anisotropic local field mechanism on the HD-vSFG spectrum of the air/water interface. It should also be noted that local DFT functionals such as those used in refs 36 and 52 predict extremely large deviations (as large as 400−500 cm^{-1}) from the reference values for the vibrational frequencies of water clusters[54] which effectively prevents a direct comparison between the experimental and calculated HD-vSFG spectra without relying on ad hoc approximations.

To add further uncertainty to the molecular-level characterization of the air/water interface, new measurements of $\mathrm{Im}[\chi^{(2,R)}_{xxz}(\omega)]$ based on an accurate examination of the phase as well as amplitude calibration using different nonresonant materials have concluded that the HD-vSFG spectrum of the air/water interface does not display any noticeable positive feature in the low-frequency hydrogen-bonded region.[41] It should be noted that the absence of the positive feature at ∼3100 cm^{-1} was also found in the HD-vSFG spectrum measured using a newly developed picosecond heterodyne scheme.[40] The measurements of refs 40 and 41 suggest that the OH(x) band observed in previous experiments arises from artifacts associated with inaccuracies in the phase determination and the use of crystalline quartz as the reference material. These new experimental results call into question the current understanding of the molecular structure of the air/water interface derived from the analysis of previously measured and simulated HD-vSFG spectra. From a theoretical standpoint, a correct modeling of the HD-vSFG spectrum requires an accurate representation of the multidimensional potential energy, dipole moment, and polarizability surfaces in combination with a quantum mechanical treatment of the molecular motion. Although some of these components were either neglected or only taken into account in an approximate fashion in previous simulations,[30,32,33,36,52] they are rigorously included in the MB-MD simulations described in this study.

RESULTS AND DISCUSSION

The HD-vSFG spectrum in the SSP polarization combination calculated from quantum MB-MD simulations within the centroid molecular dynamics (CMD) formalism[55] is shown in Figure 1 along with the corresponding experimental results from refs 33 and 41. Good agreement is obtained between simulation and experiment without requiring any empirical frequency shift or ad hoc scaling of the HD-vSFG intensity. The accuracy exhibited by the CMD HD-vSFG spectrum demonstrates the importance of nuclear quantum effects, neglected in all previous theoretical studies, for correctly determining the structural arrangements of the water molecules at the interface and provides further evidence for the predictive power of quantum MB-MD simulations with the MB-pol potential for characterizing the properties of water across different phases.

Because the CMD MB-MD simulations rigorously describe all contributions to the HD-vSFG response in eq 1 (e.g., many-body interactions, electric polarization, and nuclear quantum effects), the direct comparison between the experimental and calculated spectra provides the unique opportunity to dissect systematically the different spectral features in terms of their molecular origins. First, it is possible to note that although the frequency range of the free OH peak (∼3700 cm^{-1}) is well-reproduced in the CMD HD-vSFG spectrum the peak is noticeably broader than that in the experimental spectrum. This is a typical manifestation of the so-called "curvature problem"

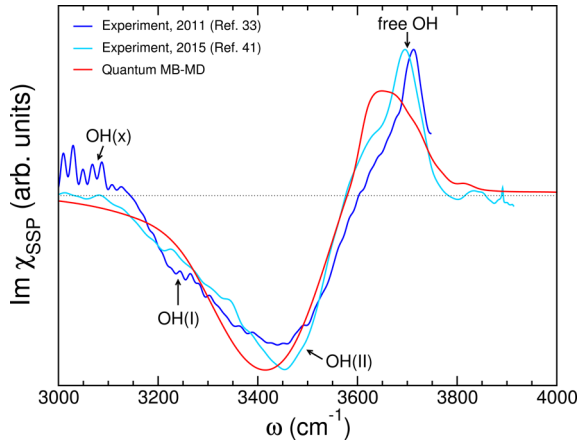

Figure 1. Comparison between the experimental and quantum HD-vSFG spectra of the air/water interface. The quantum HD-vSFG spectrum (shown in red) was obtained from MB-MD simulations carried out within the CMD formalism. The truncated cross-correlation function, without including explicit short-range two-body contributions to the total dipole moment and polarizability, was used to solve eq 1. The experimental spectra from refs 33 and 41 are shown in dark and light blue, respectively, along with labels for the more relevant features discussed in the text.

associated with the CMD formalism.[56] Although this deficiency was shown to be negligible in CMD simulations of vibrational spectra of liquid water at ambient conditions,[57,58] the curvature problem is clearly manifest in CMD calculations of the vibrational frequencies of a water molecule in the gas phase, which closely resemble the vibrational frequencies of dangling OH bonds of water molecules at the air/water interface. As discussed in detail in ref 58, no simulation approach currently exists that is capable of exactly capturing the quantum behavior of high-frequency and anharmonic vibrations in molecular systems with many degrees of freedom.

Although the CMD HD-vSFG spectrum accurately reproduces both the negative intensity and width of the hydrogen-bonded band between 3200 and 3600 cm^{-1}, which was not correctly represented in previous simulations (Figures 3 and 4), no well-resolved OH(I) feature is discernible at ∼3250 cm^{-1}. This feature, which is absent from the most recent measurements,[41] has been attributed to intramolecular anharmonic coupling.[33] The present quantum MB-MD simulations thus offer some insight into the physical mechanisms responsible for the OH(I) spectral feature. As previously demonstrated,[46] CMD MB-MD simulations are unable to capture quantitatively higher-order quantum dynamical effects (e.g., association bands and Fermi resonances) in the IR and Raman spectra of liquid water. Therefore, although the CMD HD-vSFG spectrum of the air/water interface at ∼3250 cm^{-1} is in agreement with the recent measurements reported in ref 41, the absence of the OH(I) feature is also consistent with the assignment of this feature to intramolecular vibrational coupling.[33] Finally, no positive feature is present in the low-frequency hydrogen-bonded region (∼3100 cm^{-1}) of the CMD HD-vSFG spectrum, in agreement with the most recent experimental measurements[40,41] but at variance with previous experimental[29,33] and simulation studies.[30,32]

To provide a quantitative interpretation of the different spectral features in connection with the underlying structure of the air/water interface, the CMD HD-vSFG spectrum is systematically dissected in terms of its fundamental contribu-

DOI: 10.1021/jacs.6b00893
J. Am. Chem. Soc. 2016, 138, 3912−3919

tions, starting from the role played by nuclear quantum effects. To this end, the HD-vSFG spectrum in the SSP polarization combination calculated from classical MB-MD simulations is shown in Figure 2 along with the corresponding experimental results from refs 33 and 41.

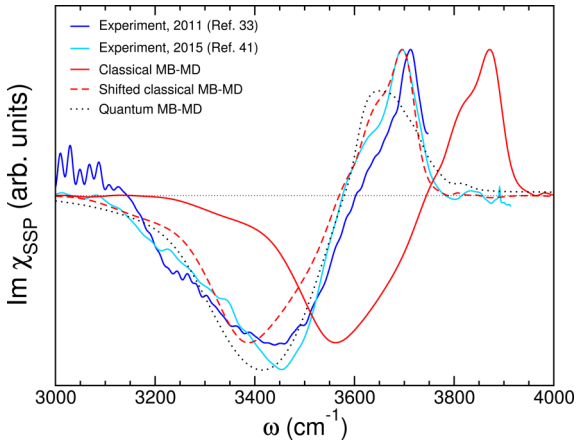

Figure 2. Comparison between the experimental and calculated HD-vSFG spectra of the air/water interface. The continuous red trace corresponds to the HD-vSFG spectrum calculated according to eq 1 from classical MB-MD simulations with the MB-pol water potential using the full MB-μ many-body representation of the total dipole moment along with the one- and two-body terms of the MB-α representation of the total polarizability.[46] Also shown as a dashed red trace is the classical HD-vSFG spectrum shifted by 175 cm^{-1} to approximately account for nuclear quantum effects. (See the Supporting Information.) The experimental HD-vSFG spectra from refs 33 and 41 are shown in dark and light blue, respectively. Also shown (dotted black line) for comparison is the quantum (CMD) HD-vSFG spectrum presented in Figure 1.

The comparison of the classical and CMD HD-vSFG spectra shown in Figure 2 indicates that the neglect of nuclear quantum effects results in an effectively rigid blueshift of 175 cm^{-1} of all spectral features. A similar blueshift is also obtained from the frequency difference between the positions of the OH vibrational band predicted by classical and CMD simulations of the infrared spectrum of bulk water. (See the Supporting Information for specific details.) The magnitude of the frequency shift can thus be explained by considering the interplay between zero-point energy effects and anharmonicity associated with the OH stretching vibrations. Interestingly, the classical HD-vSFG spectrum clearly displays the shoulder of the free OH peak (~3640 cm^{-1}), which reinforces the notion that the absence of this feature in the quantum spectrum can be attributed to the CMD curvature problem. This shoulder has been assigned to the asymmetric stretching mode of interfacial water molecules.[31,42]

Upon shifting the classical HD-vSFG spectrum to the red by 175 cm^{-1} (dashed red line in Figure 2), there is almost a one-to-one correspondence with the CMD HD-vSFG spectrum. The most notable difference is the reduced negative intensity on the right side (~3500 cm^{-1}) of the classical hydrogen-bonded band, which is the frequency region associated with weak hydrogen bonds. This difference can be explained by considering that the neglect of nuclear quantum effects in water leads to a more structured liquid characterized by relatively stronger hydrogen bonds.[45,59] As in the CMD HD-vSFG spectrum, the OH(I) feature is absent from the corresponding classical results, with the intensity dying off more quickly than that of experiment in the region from 3200−3350 cm^{-1}, in agreement with the most recent measurements of the HD-vSFG spectrum.[41] However, it should be noted that because classical simulations are not capable of capturing the intramolecular Fermi resonance due in part to the mismatch between the classical frequencies of the water bending overtone and stretching vibrations the absence of the OH(I) feature is also consistent with its assignment to intramolecular anharmonic coupling.[33] Importantly, the classical HD-vSFG spectrum does not exhibit any noticeable positive feature in the low-frequency hydrogen-bonded region (~3100 cm^{-1}), in agreement with the CMD HD-vSFG spectrum and more recent experimental measurements. The similarity between the shifted classical and quantum spectra at ~3100 cm^{-1} indicates that dynamical effects are not responsible for establishing interfacial water structures with dipole moments pointing toward the air phase, which would lead to a positive feature in the HD-vSFG spectra.

Further insights into the molecular origin of the individual spectral features can be derived from the analysis of both electrostatic and structural contributions to the simulated HD-vSFG spectrum. Considering the computational cost associated with the CMD simulations and the similarity between the (shifted) classical and quantum results, this analysis is carried out for the classical HD-vSFG spectrum only. In Figure 3, the (shifted) classical MB-MD HD-vSFG spectrum is decomposed in terms of the many-body contributions to the electrostatic

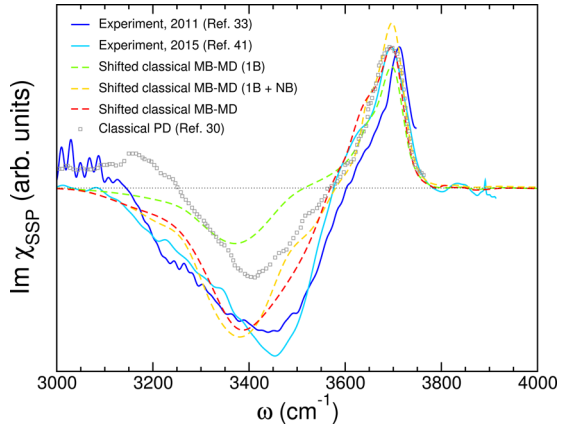

Figure 3. Decomposition of the HD-vSFG spectrum of the air/water interface in terms of the many-body components of the total dipole moment and polarizability calculated according to eq 1 from classical MB-MD simulations with the MB-pol water potential. The dashed green trace corresponds to the HD-vSFG spectrum obtained when only one-body (1B) contributions to the total dipole moment and polarizability are included in the calculation of the time-correlation function in eq 1. The dashed yellow trace corresponds to the HD-vSFG spectrum when both one- and N-body (1B + NB) but not explicit short-range two-body contributions to the total dipole moment along with 1B contributions to the total polarizability are included in the calculation of the time-correlation function in eq 1. The dashed red trace corresponds to the full classical MB-MD HD-vSFG spectrum shown in Figure 2. As in Figure 2, all classical spectra are shifted by −175 cm^{-1} to approximately account for nuclear quantum effects. (See Supporting Information.) The experimental HD-vSFG spectra from refs 33 and 41 are shown in dark and light blue, respectively. Also shown for comparison is the classical HD-vSFG spectrum calculated from simulations with the point polarizable dipole model (PD) of ref 30

DOI: 10.1021/jacs.6b00893
J. Am. Chem. Soc. 2016, 138, 3912−3919

properties. When the total dipole moment and polarizability are approximated by a sum of the corresponding one-body gas-phase values (i.e., when induction effects arising from interactions between individual molecules are neglected), the overall intensity of the hydrogen-bonded band at 3200−3600 cm^{-1} is reduced appreciably relative to that of the free OH peak (green trace). These results clearly demonstrate the gas-phase character of the dangling OH bonds and the cooperative nature of the electrostatic properties of the (interfacial) hydrogen-bond network. The inclusion of many-body contributions, either with (red trace) and without (yellow trace) explicitly taking into account short-range two-body electrostatic effects, is clearly necessary to recover correctly the experimental (negative) intensity. This is consistent with the observed enhancement of the IR intensity of the water stretching vibrations going from the gas to the liquid phase, which results from many-body effects causing large changes to the molecular dipole moments during OH vibrations within the hydrogen-bond network. The comparison between the red and yellow traces in Figure 3 allows for an assessment of the impact of short-range two-body dipoles on the line shape. Although these contributions, which are most important for strongly hydrogen bonded molecules, have been shown to significantly alter the intensity of the IR spectrum of liquid water,[47] the small differences between the red and yellow traces demonstrate that these effects play a marginal role in determining the overall shape of the HD-vSFG spectrum of the air/water interface.

As discussed in the "Brief Overview" section, short-range two-body contributions to the water dipole moment were proposed to give rise to the positive OH(x) feature at ∼3100 cm^{-1} through the anisotropic local field mechanism.[30] It should be noted that the positive feature at ∼3100 cm^{-1} was absent in the HD-vSFG spectrum calculated in ref 30 using the original charge response kernel (CRK) model and could only be recovered after modifying the description of the short-range induction contributions to the dipole moments of the water molecules (the PD model, Figure 3). However, the reparametrization of the short-range electrostatic interactions was carried out at the DFT level using B3LYP data, which have been shown to deviate significantly from correlated electronic structure reference calculations.[46] In contrast, the two-body part of the MB-MD dipole moment was derived from second-order Møller−Plesset perturbation theory (MP2) data, which closely reproduce results obtained at the coupled cluster level including single, double, and iterative triple excitations (i.e., CCSD(T), the current "gold standard" in electronic structure calculations of water interactions).[60] The shifted classical HD-vSFG spectra presented in Figure 3 thus show that two-body dipoles slightly modify the intensity between 3200−3600 cm^{-1} but clearly do not lead to any positive signal in the low-frequency portion of the hydrogen-bonded band. Therefore, the appearance of the positive feature in the low-frequency region of the hydrogen-bonded band of the HD-vSFG spectrum calculated in ref 30 with the modified electrostatic interactions is likely associated with inaccuracies in the representation of the two-body contributions to the water dipole moments.

Other theoretical investigations of the HD-vSFG spectrum have focused on the role of short-range three-body interactions in altering the hydrogen-bond network at the air/water interface. Specifically, an explicit treatment of three-body interactions was found in ref 32 to give rise to the positive OH(x) feature in the low-frequency hydrogen-bonded region of the HD-vSFG spectrum. To test this hypothesis with the more accurate MB-pol water potential and investigate how different structural arrangements of water molecules in the interface region can affect the HD-vSFG spectrum, additional classical MB-MD simulations were carried out in which three-body interactions were only taken into account in a mean-field fashion through many-body induction (i.e., without including explicit short-range three-body effects). The resulting MB-MD HD-vSFG spectra calculated with (red trace) and without (green trace) short-range three-body contributions are compared in Figure 4. Although both traces exhibit similar

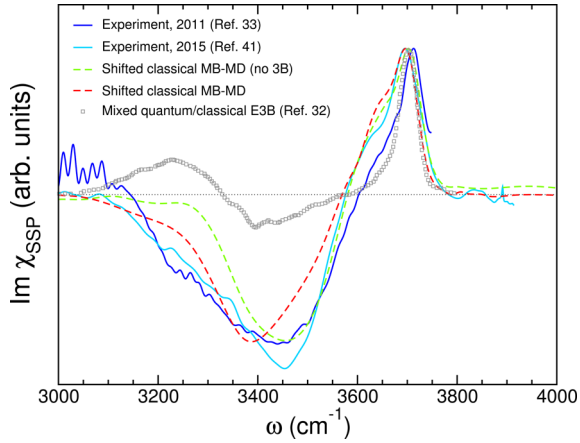

Figure 4. Decomposition of the HD-vSFG spectrum of the air/water interface in terms of the many-body components of the total interaction energy. The dashed green trace corresponds to the HD-vSFG spectrum obtained by neglecting short-range three-body contributions to the global MB-pol potential energy surface.[44] The dashed red trace corresponds to the full classical MB-MD HD-vSFG spectrum shown in Figure 2. As in Figure 2, all classical spectra are shifted by −175 cm^{-1} to approximately account for nuclear quantum effects. The experimental HD-vSFG spectra from refs 33 and 41 are shown in dark and light blue, respectively. Also shown for comparison is the mixed quantum/classical HD-vSFG spectrum obtained with the empirical E3B model in ref 32.

overall shapes, significant differences exist in the hydrogen-bonded region, with the neglect of short-range three-body effects increasing the intensity corresponding to weakly hydrogen-bonded configurations (∼3450 cm^{-1}) while decreasing the intensity associated with more strongly hydrogen-bonded configurations (∼3250 cm^{-1}).

The influence of short-range three-body effects on the HD-vSFG spectrum can be understood from the analysis of the structure of the water hydrogen-bond network in the interfacial region. Employing the definition of instantaneous interfaces introduced in ref 61 to isolate the outermost layer of water molecules that dominate the HD-vSFG spectrum, the hydrogen bonding environment of each molecule was determined on the basis of the number of hydrogen bonds donated and accepted by each molecule. Consistent with the HD-vSFG spectra in Figure 4, it is found that the percentage of weaker tetrahedrally coordinated molecules within one molecular layer of the instantaneous interface increases (from 16.7 to 19.6%) and the number of more strongly hydrogen-bonded pairs decreases (from 37.8 to 34.8%) when the accurate short-range three-body interactions of MB-pol are replaced with a mean-field treatment. Further details on the hydrogen-bonding structure at the interface are presented in the Supporting Information.

DOI: 10.1021/jacs.6b00893
J. Am. Chem. Soc. 2016, 138, 3912−3919

Although these results are somewhat consistent with the molecular interpretation proposed in ref 32 from simulations with a relatively simple E3B water model, MB-MD simulations performed with the more accurate MB-pol potential demonstrate that although three-body contributions are necessary to predict the correct intensity of the hydrogen-bonded band three-body interactions are not responsible for the positive feature observed in the measurements of refs 29 and 33. The appearance of the positive feature at ∼3100 cm^{-1} in the simulated HD-vSFG spectrum of ref 32 is thus likely due to inaccuracies in the representation of three-body effects within the E3B model as previously reported from a systematic analysis of the many-body expansion of the water interaction energy.[62]

CONCLUSIONS

In this study, we have reported the first quantum simulations of the HD-vSFG spectrum of the air/water interface performed with the recently developed MB-MD methodology. For the first time, excellent agreement between the theoretical predictions and experimental measurements is found without requiring any empirical frequency shift or ad hoc scaling of the HD-vSFG intensity of the calculated spectrum. Importantly, a systematic analysis of the MD-MB results has allowed for a quantitative dissection of the calculated spectrum in terms of distinct contributions from electrostatic, structural, and nuclear quantum effects, providing a definitive molecular-level description of the air/water interface. In particular, the MB-MD results, summarized in Figure 5, demonstrate that short-range electrostatic interactions between (strongly) hydrogen-bonded pairs of molecules as well as short-range three-body contributions to the underlying intermolecular interactions are key to establishing a molecular structure of the interface region consistent with the experimental spectra. However, contrary to previous simulation studies,[32,33] these contributions are shown to not be responsible for any noticeable positive feature in the low-frequency hydrogen-bonded region of the spectrum. The explicit treatment of nuclear quantum effects in the simulations is demonstrated to be necessary for a quantitative reproduction of the most recent experimental measurements.[40,41] The absence of the positive OH(x) band at ∼3100 cm^{-1} in the quantum HD-vSFG spectrum calculated from the MB-MD simulations supports the assignment of this feature to experimental artifacts associated with inaccuracy in the phase determination and the use of crystalline quartz as the reference material.[40,41] Besides revealing the molecular structure of the air/water interface, the agreement between the theoretical and experimental spectra demonstrates the predictive power of the MB-MD simulations to gain fundamental insights into the microscopic properties of aqueous interfaces, such as those between ionic solutions and both biological and metal surfaces, which will be the focus of future studies.

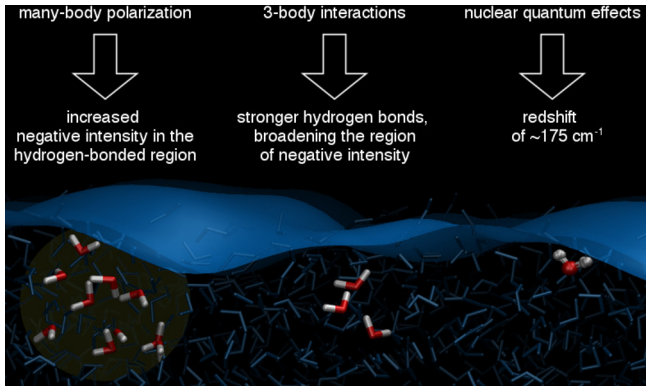

Figure 5. Schematic illustration of the different contributions to the HD-vSFG spectrum of the air/water interface in the OH stretching region (3000−3800 cm^{-1}).

METHODS

In all MB-MD simulations, the water interactions were described by the many-body MB-pol water potential, which provides an accurate description of the properties of water from the gas to the condensed phase.[43−47] The classical MB-MD simulations were carried out for a system consisting of 512 molecules in a simulation box with dimensions 26 × 26 × 100 $Å^3$ in 3D periodic boundary conditions, with the water molecules forming a stable slab parallel to the xy plane. The slab system was equilibrated at 298.15 K in the canonical (NVT: constant number of molecules, volume, temperature) ensemble. The equations of motion were propagated using the velocity−Verlet algorithm with a time step Δt = 0.2 fs, and the temperature was controlled via Nosé−Hoover chains of four thermostats coupled to each degree of freedom.[63] Classical MB-MD simulations predict a surface tension for the MB-pol potential of 68 ± 2 mJ m^{-2}, in good agreement with the experimental value of 71.73 mJ m^{-2}. Over the course of a 2.5 ns NVT simulation, 415 independent initial conditions were extracted. For each initial condition, a 50 ps simulation in the microcanonical (NVE: constant number of molecules, volume, energy) ensemble was performed. The resulting ∼20 ns of NVE trajectories were used to calculate the time-correlation function entering the expression for the imaginary part of $\chi^{(2,R)}$ in the SSP polarization (eq 1). The SSP time-correlation function was calculated as

$$\frac{\langle \alpha_{xx}(t)\mu_z(0)\rangle + \langle \alpha_{yy}(t)\mu_z(0)\rangle}{2} \quad (2)$$

where z was defined perpendicular to the interface and the time-correlation functions arising from the xx and yy components of the polarizability were averaged to exploit the symmetry in the plane of the air/water interface. Because of the slab configuration, the z component of the dipole moment for molecules in the lower half of the slab was mirrored following the protocol of ref 64. Although the full MB-μ dipole moment surface[46] including all many-body effects was used in the calculations presented in Figure 2, only the one- and two-body terms of the MB-α many-body polarizability surface[46] were included in the representation of the total polarizability. It has been shown that this approximation only impacts the overall intensity of the spectral features but not the actual lineshapes.[46] Therefore, because the HD-vSFG spectra are reported in arbitrary units, neglecting higher-order contributions to the total polarizability does not affect the interpretation of the spectral features. To analyze individual electrostatic contributions to the classical HD-vSFG spectrum, different approximations to the total dipole moment and polarizability were used in the calculation of the time-correlation function of eq 2. Specifically, in Figure 3, the classical HD-vSFG spectrum was also calculated including only one-body (i.e., gas-phase monomer) contributions to the total dipole moment and polarizability (green trace labeled as "1B") as well as neglecting explicit short-range two-body contributions to the total dipole moment (yellow trace labeled as "1B + NB").

Because of the associated computational cost, the CMD MB-MD simulations were carried out using a slightly reduced system of 310 molecules in a rectangular simulation box with dimensions 22 × 22 × 100 $Å^3$ in 3D periodic boundary conditions. Because the high-frequency region of the HD-vSFG spectrum probes local vibrational dynamics associated with the OH stretching modes, the reduced system size is expected to have a negligible effect on the calculated spectral features. The slab system was initially equilibrated for 100 ps at 298 K under NVT ensemble using path-integral molecular dynamics

DOI: 10.1021/jacs.6b00893
J. Am. Chem. Soc. 2016, 138, 3912−3919

(PIMD).[65,66] Over the course of an additional 300 ps of a PIMD simulation, 25 independent instantaneous configurations of the system were extracted to serve as initial conditions for subsequent CMD simulations. Similarly to ref 46, the CMD propagation was performed in the normal-mode representation in which the dynamics of the centroid and nonzero frequency normal modes were decoupled using an adiabaticity parameter $\gamma = 0.15$.[55] Each CMD trajectory was run for 50 ps, and a time step of 0.05 fs was found to be sufficient for energy conservation. Because of the limited CMD sampling (1.25 ns total), the quantum HD-vSFG spectrum was calculated using a truncated cross-correlation function (TCF), which includes correlations between the dipole moment and polarizability on the same molecule as well as on neighboring molecules within a predefined cutoff distance.[64] Specific details about the CMD simulations and the TCF approximation are reported in the Supporting Information.

■ ASSOCIATED CONTENT

Supporting Information

The Supporting Information is available free of charge on the ACS Publications website at DOI: 10.1021/jacs.6b00893.

Comparison between classical and quantum MB-MD simulations of the IR spectrum of liquid water. Comparison between the HD-vSFG spectra calculated using different approximations to the time-correlation function of eq 1. Analysis of the hydrogen-bonding structure at the air/water interface. (PDF)

■ AUTHOR INFORMATION

Corresponding Author

*E-mail: fpaesani@ucsd.edu

Notes

The authors declare no competing financial interest.

■ ACKNOWLEDGMENTS

We thank Dr. Volodymyr Babin for his contribution to the initial development of many-body molecular dynamics and for his design of the TOC graphic. We also thank Prof. Adam Willard for his guidance on the calculations of the instantaneous air/water interface, Dr. Yuki Nagata and Prof. Mischa Bonn for helpful discussions on the interpretation of HD-vSFG spectra, and Prof. Tahei Tahara for providing the experimental data of refs 33 and 41. This research was supported by the National Science Foundation through grant numbers CHE-1453204 and CHE-1305427 ("CCI: Center for Aerosol Impacts on Climate and the Environment"). This work used the Extreme Science and Engineering Discovery Environment (XSEDE), which is supported by the National Science Foundation grant number ACI-1053575 (allocation TG-CHE110009). G.R.M. acknowledges the Department of Education for support through the GAANN fellowship program.

■ REFERENCES

(1) Pratt, L. R.; Pohorille, A. *Chem. Rev.* **2002**, *102*, 2671−2692.
(2) Richmond, G. L. *Chem. Rev.* **2002**, *102*, 2693−2724.
(3) Eisenthal, K. B. *Chem. Rev.* **2006**, *106*, 1462−1477.
(4) Jungwirth, P.; Tobias, D. J. *Chem. Rev.* **2006**, *106*, 1259−1281.
(5) Johnson, C. M.; Baldelli, S. *Chem. Rev.* **2014**, *114*, 8416−8446.
(6) Bonn, M.; Nagata, Y.; Backus, E. H. G. *Angew. Chem., Int. Ed.* **2015**, *54*, 5560−5576.
(7) Knipping, E. M.; Lakin, M. J.; Foster, K. L.; Jungwirth, P.; Tobias, D. J.; Gerber, R. B.; Dabdub, D.; Finlayson-Pitts, B. J. *Science* **2000**, *288*, 301−306.
(8) Davidovits, P.; Kolb, C. E.; Williams, L. R.; Jayne, J. T.; Worsnop, D. R. *Chem. Rev.* **2006**, *106*, 1323−1354.
(9) Prather, K. A.; Bertram, T. H.; Grassian, V. H.; Deane, G. B.; Stokes, M. D.; DeMott, P. J.; Aluwihare, L. I.; Palenik, B. P.; Azam, F.; Seinfeld, J. H.; Moffet, R. C.; Molina, M. J.; Cappa, C. D.; Geiger, F. M.; Roberts, G. C.; Russell, L. M.; Ault, A. P.; Baltrusaitis, J.; Collins, D. B.; Corrigan, C. E.; Cuadra-Rodriguez, L. A.; Ebben, C. J.; Forestieri, S. D.; Guasco, T. L.; Hersey, S. P.; Kim, M. J.; Lambert, W. F.; Modini, R. L.; Mui, W.; Pedler, B. E.; Ruppel, M. J.; Ryder, O. S.; Schoepp, N. G.; Sullivan, R. C.; Zhao, D. *Proc. Natl. Acad. Sci. U. S. A.* **2013**, *110*, 7550−7555.
(10) Levy, Y.; Onuchic, J. N. *Annu. Rev. Biophys. Biomol. Struct.* **2006**, *35*, 389−415.
(11) Killian, J.; von Heijne, G. *Trends Biochem. Sci.* **2000**, *25*, 429−434.
(12) Pal, S. K.; Zhao, L.; Zewail, A. H. *Proc. Natl. Acad. Sci. U. S. A.* **2003**, *100*, 8113−8118.
(13) Pal, S.; Maiti, P. K.; Bagchi, B.; Hynes, J. T. *J. Phys. Chem. B* **2006**, *110*, 26396−26402.
(14) Carrasco, J.; Hodgson, A.; Michaelides, A. *Nat. Mater.* **2012**, *11*, 667−674.
(15) Limmer, D. T.; Willard, A. P.; Madden, P.; Chandler, D. *Proc. Natl. Acad. Sci. U. S. A.* **2013**, *110*, 4200−4205.
(16) Ghosal, S.; Hemminger, J. C.; Bluhm, H.; Mun, B. S.; Hebenstreit, E. L. D.; Ketteler, G.; Ogletree, D. F.; Requejo, F. G.; Salmeron, M. *Science* **2005**, *307*, 563−566.
(17) Taylor, D. J. F.; Thomas, R. K.; Penfold, J. *Langmuir* **2002**, *18*, 4748−4757.
(18) Mojet, B. L.; Ebbesen, S. D.; Lefferts, L. *Chem. Soc. Rev.* **2010**, *39*, 4643−4655.
(19) Perry, A.; Neipert, C.; Space, B.; Moore, P. B. *Chem. Rev.* **2006**, *106*, 1234−1258.
(20) Byrnes, S. J.; Geissler, P. L.; Shen, Y. *Chem. Phys. Lett.* **2011**, *516*, 115−124.
(21) Kawaguchi, T.; Shiratori, K.; Henmi, Y.; Ishiyama, T.; Morita, A. *J. Phys. Chem. C* **2012**, *116*, 13169−13182.
(22) Shen, Y. R. *Nature* **1989**, *337*, 519−525.
(23) Shen, Y. R.; Ostroverkhov, V. *Chem. Rev.* **2006**, *106*, 1140−1154.
(24) Du, Q.; Superfine, R.; Freysz, E.; Shen, Y. R. *Phys. Rev. Lett.* **1993**, *70*, 2313−2316.
(25) Du, Q.; Freysz, E.; Shen, Y. R. *Science* **1994**, *264*, 826−828.
(26) Kuo, I.-F. W.; Mundy, C. J. *Science* **2004**, *303*, 658−660.
(27) Ostroverkhov, V.; Waychunas, G. A.; Shen, Y. R. *Phys. Rev. Lett.* **2005**, *94*, 046102.
(28) Sovago, M.; Campen, R. K.; Wurpel, G. W. H.; Müller, M.; Bakker, H. J.; Bonn, M. *Phys. Rev. Lett.* **2008**, *100*, 173901.
(29) Tian, C.-S.; Shen, Y. *J. Am. Chem. Soc.* **2009**, *131*, 2790−2791.
(30) Ishiyama, T.; Morita, A. *J. Chem. Phys.* **2009**, *131*, 244714.
(31) Stiopkin, I. V.; Weeraman, C.; Pieniazek, P. A.; Shalhout, F. Y.; Skinner, J. L.; Benderskii, A. V. *Nature* **2011**, *474*, 192−195.
(32) Pieniazek, P. A.; Tainter, C. J.; Skinner, J. L. *J. Am. Chem. Soc.* **2011**, *133*, 10360.
(33) Nihonyanagi, S.; Ishiyama, T.; Lee, T.; Yamaguchi, S.; Bonn, M.; Morita, A.; Tahara, T. *J. Am. Chem. Soc.* **2011**, *133*, 16875−16880.
(34) Zhang, Z.; Piatkowski, L.; Bakker, H. J.; Bonn, M. *Nat. Chem.* **2011**, *3*, 888−893.
(35) Vinaykin, M.; Benderskii, A. V. *J. Phys. Chem. Lett.* **2012**, *3*, 3348−3352.
(36) Sulpizi, M.; Salanne, M.; Sprik, M.; Gaigeot, M.-P. *J. Phys. Chem. Lett.* **2013**, *4*, 83−87.
(37) Geissler, P. L. *Annu. Rev. Phys. Chem.* **2013**, *64*, 317−337.
(38) Hsieh, C.-S.; Okuno, M.; Hunger, J.; Backus, E. H. G.; Nagata, Y.; Bonn, M. *Angew. Chem., Int. Ed.* **2014**, *53*, 8146−8149.
(39) Ishiyama, T.; Morita, A.; Tahara, T. *J. Chem. Phys.* **2015**, *142*, 212407.
(40) Yamaguchi, S. *J. Chem. Phys.* **2015**, *143*, 034202.
(41) Nihonyanagi, S.; Kusaka, R.; Inoue, K.-i.; Adhikari, A.; Yamaguchi, S.; Tahara, T. *J. Chem. Phys.* **2015**, *143*, 124707.

DOI: 10.1021/jacs.6b00893
J. Am. Chem. Soc. 2016, 138, 3912−3919

(42) Nagata, Y.; Hasegawa, T.; Backus, E. H. G.; Usui, K.; Yoshimune, S.; Ohto, T.; Bonn, M. *Phys. Chem. Chem. Phys.* **2015**, *17*, 23559−23564.
(43) Babin, V.; Leforestier, C.; Paesani, F. *J. Chem. Theory Comput.* **2013**, *9*, 5395−5403.
(44) Babin, V.; Medders, G. R.; Paesani, F. *J. Chem. Theory Comput.* **2014**, *10*, 1599−1607.
(45) Medders, G. R.; Babin, V.; Paesani, F. *J. Chem. Theory Comput.* **2014**, *10*, 2906−2910.
(46) Medders, G. R.; Paesani, F. *J. Chem. Theory Comput.* **2015**, *11*, 1145−1154.
(47) Medders, G. R.; Götz, A. W.; Morales, M. A.; Bajaj, P.; Paesani, F. *J. Chem. Phys.* **2015**, *143*, 104102.
(48) Morita, A.; Hynes, J. T. *J. Phys. Chem. B* **2002**, *106*, 673−685.
(49) Nihonyanagi, S.; Yamaguchi, S.; Tahara, T. *J. Chem. Phys.* **2009**, *130*, 204704.
(50) Nihonyanagi, S.; Mondal, J. A.; Yamaguchi, S.; Tahara, T. *Annu. Rev. Phys. Chem.* **2013**, *64*, 579−603.
(51) Wan, Q.; Galli, G. *Phys. Rev. Lett.* **2015**, *115*, 246404.
(52) Ohto, T.; Usui, K.; Hasegawa, T.; Bonn, M.; Nagata, Y. *J. Chem. Phys.* **2015**, *143*, 124702.
(53) Hasegawa, T.; Tanimura, Y. *J. Phys. Chem. B* **2011**, *115*, 5545−53.
(54) Howard, J. C.; Enyard, J. D.; Tschumper, G. S. *J. Chem. Phys.* **2015**, *143*, 214103.
(55) Voth, G. *Adv. Chem. Phys.* **1996**, *93*, 135−218.
(56) Witt, A.; Ivanov, S. D.; Shiga, M.; Forbert, H.; Marx, D. *J. Chem. Phys.* **2009**, *130*, 194510.
(57) Paesani, F.; Voth, G. A. *J. Chem. Phys.* **2010**, *132*, 014105.
(58) Rossi, M.; Liu, H.; Paesani, F.; Bowman, J.; Ceriotti, M. *J. Chem. Phys.* **2014**, *141*, 181101.
(59) Paesani, F.; Voth, G. A. *J. Phys. Chem. B* **2009**, *113*, 5702−5719.
(60) Medders, G. R.; Paesani, F. *J. Chem. Theory Comput.* **2013**, *9*, 4844−4852.
(61) Willard, A. P.; Chandler, D. *J. Phys. Chem. B* **2010**, *114*, 1954−1958.
(62) Medders, G. R.; Babin, V.; Paesani, F. *J. Chem. Theory Comput.* **2013**, *9*, 1103−1114.
(63) Martyna, G. J.; Klein, M. L.; Tuckerman, M. *J. Chem. Phys.* **1992**, *97*, 2635−2643.
(64) Nagata, Y.; Hsieh, C.-S.; Hasegawa, T.; Voll, J.; Backus, E. H. G.; Bonn, M. *J. Phys. Chem. Lett.* **2013**, *4*, 1872−1877.
(65) Chandler, D.; Wolynes, P. G. *J. Chem. Phys.* **1981**, *74*, 4078−4095.
(66) Parrinello, M.; Rahman, A. *J. Chem. Phys.* **1984**, *80*, 860−867.

DOI: 10.1021/jacs.6b00893
J. Am. Chem. Soc. 2016, 138, 3912−3919